PARTIALLY COHERENT FIELDS IN SYNTHETIC OPTICAL HOLOGRAPHY

BY

BENJAMIN PATRICK CAHILL

THESIS

Submitted in partial fulfillment of the requirements
for the degree of Master of Science in Electrical and Computer Engineering
in the Graduate College of the
University of Illinois at Urbana-Champaign, 2016

Urbana, Illinois

Adviser:

Professor P. Scott Carney

Abstract

Synthetic optical holography is a newly proposed method for implementing phase imaging in scanning near-field optical microscopy. It combines high-speed phase imaging, technical simplicity, and simultaneous operation at visible to terahertz frequencies to improve upon competing image acquisition processes by a factor of 50. This has led scanning near-field optical microscopy to become a powerful tool for nano-optical examination of surfaces. We aim to explore the effects of partial coherence in the illuminating and reference fields.

Acknowledgments

This thesis would not have been achieved in a timely manner without the help of several key people who have influenced me throughout my college and graduate school career.

I would like to thank my family for their support no matter where or what I ended up studying. My mom inspired me to work hard toward a goal I found such a strong passion for.

Several fellow graduate students were very dedicated in helping me learn the material throughout my time at the University of Illinois. In particular, Yang Xu and Martin Schnell were inspiring and incredibly patient with any questions I had, no matter how silly. Their kindness and ability to teach what they knew helped me immensely.

And I would like to thank my adviser, Professor P. Scott Carney, beyond words. I was honored to have him as a professor, adviser, and friend. He is a true mentor in the academic world and my personal life.

Contents

1. Introduction

Scanning near-field optical microscopy is an imaging technique that uses the information from evanescent waves to obtain resolution of a sample far higher than the diffraction limit. In aperture scanning near-field optical microscopy, a metal-coated probe collects the evanescent waves by scanning along the sample with a distance much smaller than the wavelength of the excitation light. As shown in Figure 1, the excitation light is emitted from the tapered fiber bundle in the probe and scatters from the sample. The particular light that interacts with both the sample and metal coat of the probe is measured and permits calculation of high spectral, spatial, and temporal resolution of the sample.

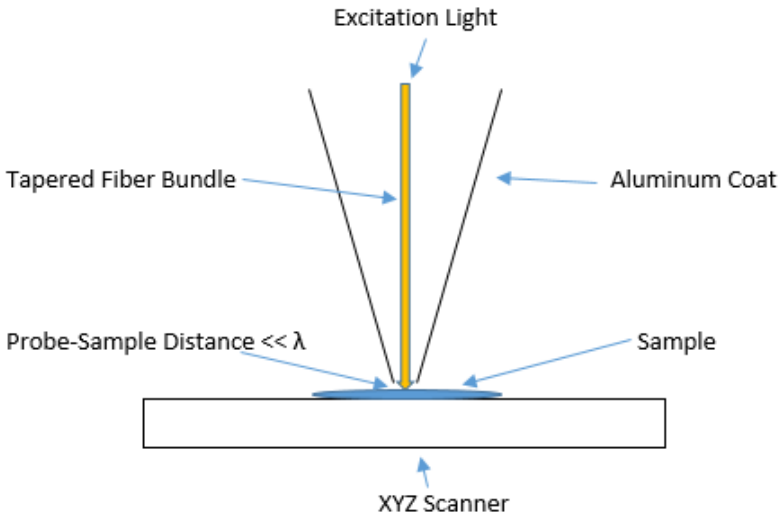

Figure 1 Aperture scanning near-field optical microscopy probe.

In apertureless scanning near-field optical microscopy, a sharp probe is placed near the sample and the light scattered from the sample via the probe tip is collected. The light from this near-field interaction must be distinguished from the light scattered by the sample directly. This is usually accomplished by locking in on the signal as the tip height is varied harmonically. Detection of a single harmonic requires interferometric detection of the optical signal to avoid cross-talk among the harmonics. This interferometry has been the bottleneck in the acquisition speed in scanning near-field optical microscopy since its inception.

Capturing the evanescent waves allows for higher resolution images than conventional microscopy systems. Normal optical systems only interpret the information from propagating waves and are thus restricted to the diffraction limit based on the wavelength of the illuminating light. The resolution of systems that exceed the diffraction limit is restricted by the ability to collect the evanescent waves. The limitation for such systems is then based on the aperture size and quality of the probe sensor rather than the wavelength of light.

In scanning near-field optical microscopy, the resolution of the sample is limited by the size of the detector aperture in aperture scanning optical microscopy or the sharpness of the tip in apertureless scanning near-field optical microscopy, and not of the wavelength of the excitation light as in normal far-field imaging. With this technique, lateral resolution of less than 20 nm and vertical resolution of 2-5 nm have been observed [1].

Contrast imaging techniques available to optical microscopy are also available to scanning near-field optical microscopy. It is possible to provide images by the contrasting fluorescence, refractive index, reflectivity, phase, differential interference, and magnetic properties, among others.

Several methods for construction of the images obtained by scanning near-field optical microscopy have been proposed. Our proposed imaging method is synthetic optical holography, which will be discussed in depth along with its advantages and applications.

Synthetic optical holography is a powerful tool in that it can provide improved image reconstruction in scanning optical near-field microscopy, as well as confocal microscopy. Confocal microscopy is an imaging technique that reconstructs three-dimensional objects by collecting images at different depths within an object. A conventional microscope can only view as far into the specimen as the light can penetrate, while a confocal microscope adds a spatial pinhole placed at the confocal plane of the lens to eliminate out-of-focus light and view one depth level at a time, enabling a highly limited and controlled depth of focus.

Synthetic optical holography is not without its limitations. The technique relies on interference effects, which diminish with partially coherent fields. We will also test the constraints of our proposed method by inputting partially coherent fields in the system, possibly introducing artifacts and limiting the use of the procedure.

2. Synthetic Optical Holography

Synthetic optical holography was introduced in 2014 [2] in the domain of near-field imaging and has since been demonstrated in confocal microscopy [3]. It has since been proposed as a method for resolving quantitative phase-resolved images in scanning near-field optical microscopy. Traditional holography is inhibited by the serial image acquisition determined by scanning optical microscopy. Synthetic optical holography enables fast computation of phase imaging, relative technical simplicity, and simultaneous operation of frequencies in the visible to terahertz range.

2.1 Background

Optical holography is an imaging method by which light scattered from an object interferes with the reference light. The resulting interference pattern contains the total complex optical field from the scattered light within a single image. This image, the hologram, allows computation of amplitude and phase images concurrently from the same data set, allowing computation times to be drastically reduced compared to other imaging strategies [2].

Camera detectors are required for wide-field holography, but the measuring of scanning near-field optical microscopy necessitates point detectors. The approach with synthetic optical holography determines the phase at each position of the image for individual pixels rather than interpreting the phase across the complete image as in wide-field holography.

Synthetic optical holography operates under the same principles as wide-field holography by interfering the scattered field, U_S, with a reference field, U_R, as shown in Figure 2a. The differences arise in the detection methods for measuring the fields. Figure 2b illustrates our specific setup of synthetic optical holography with scanning near-field optical microscopy. Notice the introduction of an atomic force microscope (AFM) for sample detection, piezo-controlled mirror (PZM) to regulate the phase of the reference field, one-pixel detector for measuring the field separately for each pixel, and the controller for closed-loop feedback of the entire system when scanning the sample [2]. (Beam splitters (BS) and mirrors (M) are also shown to explain proper beam path.)

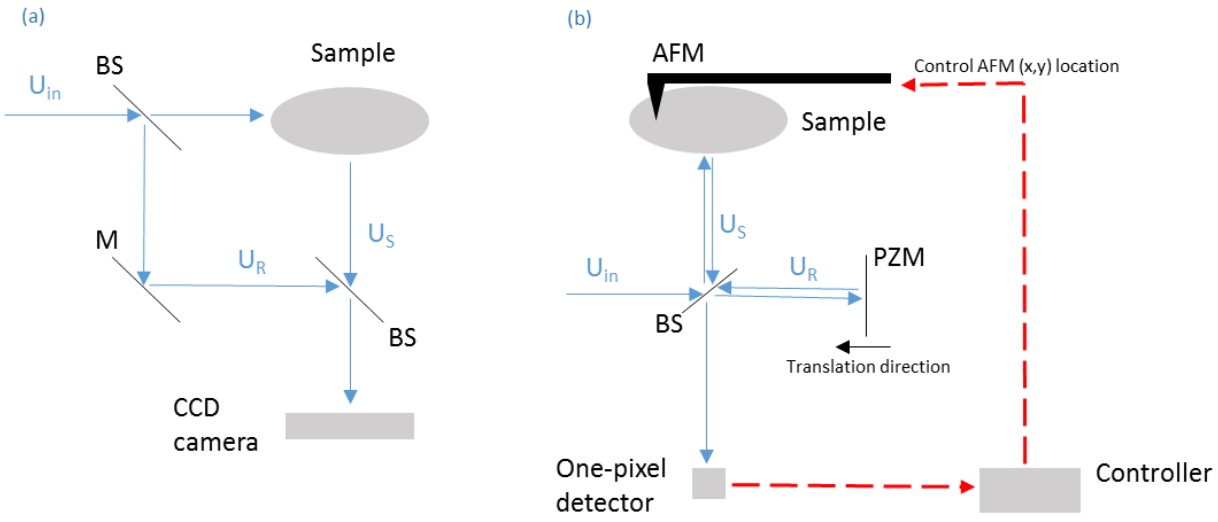

Figure 2 (a) Wide-field holography setup. (b) Synthetic optical holography setup.

Optical holography is introduced into scanning near-field optical microscopy for nanoscale resolution, structural mapping of nanomaterials, and plasmon detection in metal nanostructures. Holography has thus far not been implemented very thoroughly into scanning near-field optical microscopy, but with mutual information between image pixels, holography provides natural convenience for this application. Holography currently allows for superior contrast and spatial resolution in confocal optical microscopy.

2.2 Application

Scanning near-field optical microscopy previously used monochromatic, coherent light to illuminate a sample and an oscillating atomic force microscope to record the scattered light while scanning along the sample's surface. The atomic force microscope collects the evanescent field, which allows for resolution much greater than that of the normal diffraction limit. The detector must measure the local near field scattered by the tip while suppressing the present background fields. The scattered field interacts with the reference field and the intensity of this interference is measured by the detector. This intensity is demodulated by the specific harmonic of the oscillation frequency of the tip.

Currently in scanning near-field optical microscopy, the reference field has to be varied at each pixel to obtain background-free information. The amplitude and phase images are then resolvable. Several other imaging techniques have been proposed because of this requirement, such as heterodyne, pseudo-heterodyne, and phase-shifting interferometry [2].

At each pixel position, the scattered field is combined with the reference field at the detector. The phase of the reference field is controlled by the position of the piezo-controlled mirror that translates in the direction of the incoming field. The piezo-controlled mirror is slowly translated with respect to the rapid scanning of the probe tip over the sample surface, resulting in a quasi-constant reference phase for each pixel.

A linear mirror translation was originally chosen to show plane wave reference waves analogous to off-axis wide-field holography, yielding a simpler derivation. A sinusoidal mirror translation was decided upon next as an option when less translation space is available and to create an open-loop feedback system between probe scanning and mirror position. The nonlinear reference phase option has its advantages over linear that come at the cost of derivational complexity.

By implementing synthetic optical holography into scanning near-field microscopy, image acquisition has sped up by a factor of 50 compared to other competing imaging techniques. For the linear reference case, near-field images have been reconstructed in 26 seconds for 64 kilopixel and 13 minutes for 2.3 megapixel images [2]. This has turned scanning near-field optical microscopy into a rapid nano-imaging tool for ultra-fast nano-optical inspection of surfaces.

Synthetic optical holography could also benefit the implementation of nano-imaging in confocal microscopy, which allows dynamic optical surface examination for biological applications, semiconductor manufacturing, and micromechanical systems, among others. It is anticipated that further studies of synthetic optical holography will expose new bio-imaging applications and innovative holographic encoding and reconstruction methods.

3. Linear-Phase Reference Waves

First, we take a look into the case of reference waves changing linearly in time. The reference arm directly governs the spacing of the piezo-controlled mirror, so the PZM translating at a constant velocity forward along a stage produces a linearly changing phase in the reference wave. Since there is a physical limit to the length of the stage allowed for the PZM to move, we need to accommodate the amount of mirror travel distance for the number of pixels to be used in our detector. We present below the derivation required for the linear-phase reference case.

3.1 Derivation

In synthetic optical holography, the one-pixel detector interprets a plane wave reference field, $U_R(\boldsymbol{r})$, shown as

$$U_R(\boldsymbol{r}) = A_R e^{i\varphi_R(\boldsymbol{r})}, \tag{3.1}$$

where A_R is the reference field amplitude and

$$\varphi_R(\boldsymbol{r}) = 2\pi \cdot 2d(\boldsymbol{r})/\,\lambda \tag{3.2}$$

is the changing reference phase based on the piezo-controlled mirror position. The phase should appear quasi-static for a pixel at any given position, $d(\boldsymbol{r})$. For a reference phase changing linearly in time, the intensity measured by the detector is the same as in wide-field holography. Solving for the combined field from the scattered and reflected terms results in an intensity of

$$I(\boldsymbol{r}) = |U_R(\boldsymbol{r}) + U_S(\boldsymbol{r})|^{\,2}. \tag{3.3}$$

The complex terms are retained through the interaction, revealing

$$I(\boldsymbol{r}) = |U_R(\boldsymbol{r})|^{\,2} + |U_S(\boldsymbol{r})|^{\,2} + U_S^*(\boldsymbol{r})U_R(\boldsymbol{r}) + U_R^*(\boldsymbol{r})U_S(\boldsymbol{r}). \tag{3.4}$$

Equation (3.4) is the same as in wide-field holography for a reference phase that changes linearly in time. The amplitude and phase of the scattered field can be recovered by normal reconstruction methods. However, in synthetic optical holography, the reference field is constructed sequentially for each pixel in the image. Fourier filtering of the near-field hologram is used to reconstruct the amplitude and phase of the signal. The Fourier transform of the detected near-field hologram is

$$\tilde{I}_{p,q}(\boldsymbol{q}) = |A_R|^2\delta_{p,q} + C_{p,q}(\boldsymbol{q}) + A_R\tilde{U}^*_{S,p,q}(\boldsymbol{k}_{||} - \boldsymbol{q}) + A_R^*(\boldsymbol{r})\tilde{U}_{S,p,q}(\boldsymbol{k}_{||} + \boldsymbol{q}), \tag{3.5}$$

where a tilde indicates a Fourier transform of a variable and (p, q) are coordinates in the frequency domain.

Correct filtering in the frequency domain can reduce equation (3.5) to one term containing valuable information. The term due to the reference field, $|A_R|^2\delta_{p,q}$, is interpreted as a lone spike in the center of the frequency domain due to the Kronicker delta function. The autocorrelation term, $C_n(\boldsymbol{q})$, results from the reference field and scattered field being related with an amplitude and time shift. This is confirmed when examining the relationship in the time domain

$$U_S(t) = K(\boldsymbol{r})U_R(t), \tag{3.6}$$

where $K(\boldsymbol{r})$ is the spatial scattering term. Since

$$I(\boldsymbol{r}) = |U_S(t) + U_R(t+\tau)|^2, \tag{3.7}$$

where τ is the time delay of $U_R(t)$ due to the scattering term, then

$$I(\boldsymbol{r}) = |K(\boldsymbol{r})U_R(t) + U_R(t+\tau)|^2. \tag{3.8}$$

It is clear how the autocorrelation term is a result of the relationship between the reference and scattered fields. The term is thus a cross-correlation of the reference field and the same reference field with a time delay. The cross-correlation of a function with itself, or autocorrelation, is inherently symmetric in the frequency domain. This term is hence also located in the center of the frequency domain, however with a larger bandwidth than the Kronicker delta term.

The direct term, $A_R^*(\boldsymbol{r})\widetilde{U}_{S,p,q}(\boldsymbol{k}_{||}+\boldsymbol{q})$, and its conjugate, $A_R\widetilde{U}^*_{S,p,q}(\boldsymbol{k}_{||}-\boldsymbol{q})$, contain the same information but are inversions of each other due to a shift of $-\boldsymbol{k}_{||}$ and $\boldsymbol{k}_{||}$, respectively. By filtering out only the direct term and performing an inverse Fourier transform, we apply the correct shift of $\boldsymbol{k}_{||}$ to obtain the near-field optical amplitude and phase images, A_S and φ_S.

3.2 Verification

We confirm the use of a linear-phase reference field in synthetic optical holography as a means of reconstructing a sample image when given information about its amplitude and phase. We first construct test images to use for our simulation, as shown in Figure 3.

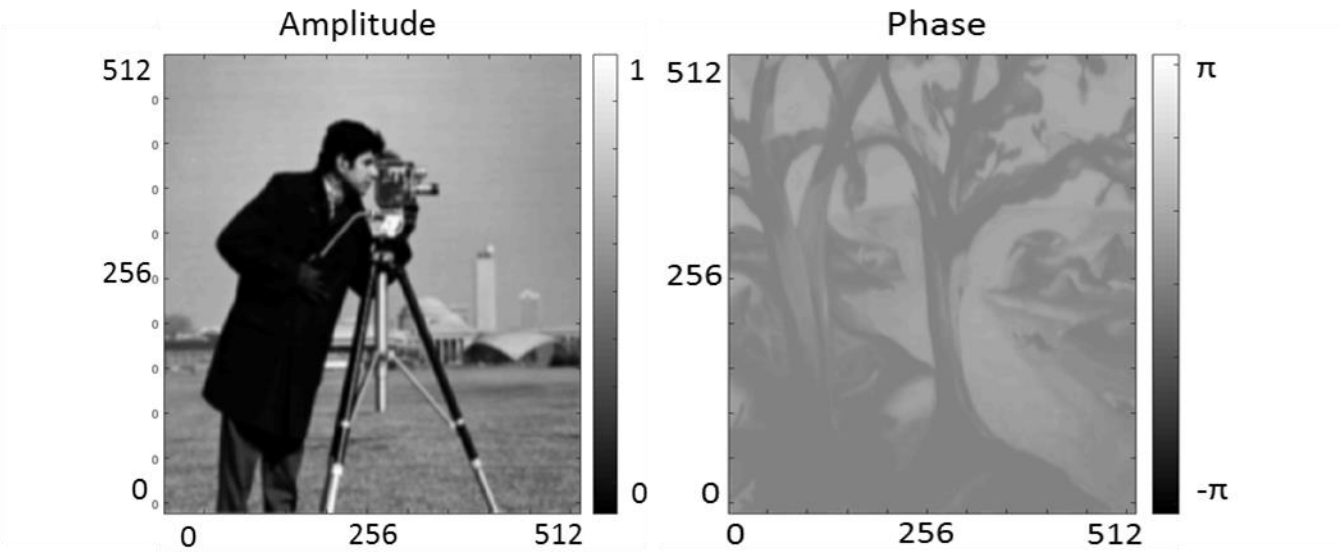

Figure 3 Original image interpreted as amplitude and phase information.

From this, we construct the reference field to have a linear phase with respect to time. The image acts as the spatial scattering term, $K(\boldsymbol{r})$, from equation (3.6) to determine the scattered field. Interfering the scattered field with the reference field results in the hologram shown in Figure 4.

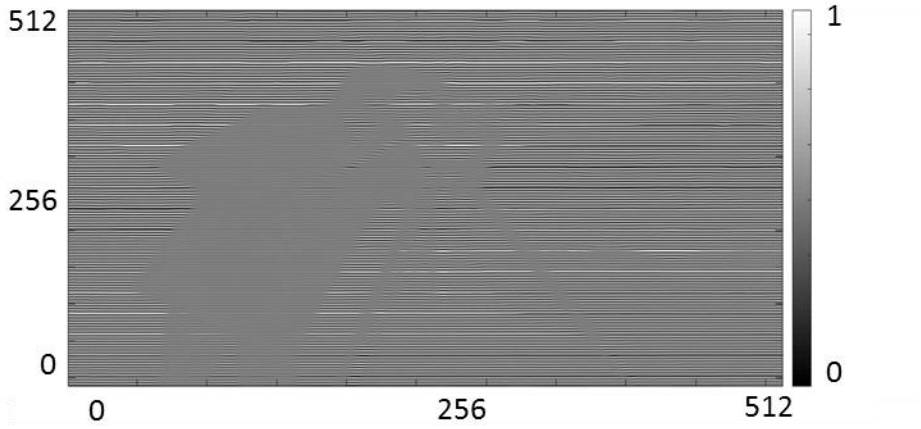

Figure 4 Hologram obtained from image and reference field.

Taking the Fourier transform of the hologram results in two discernible peaks in the frequency domain for the linear-phase reference example, as revealed in Figure 5. The central peak appears diminutive in contrast due to a comparatively large reference field amplitude.

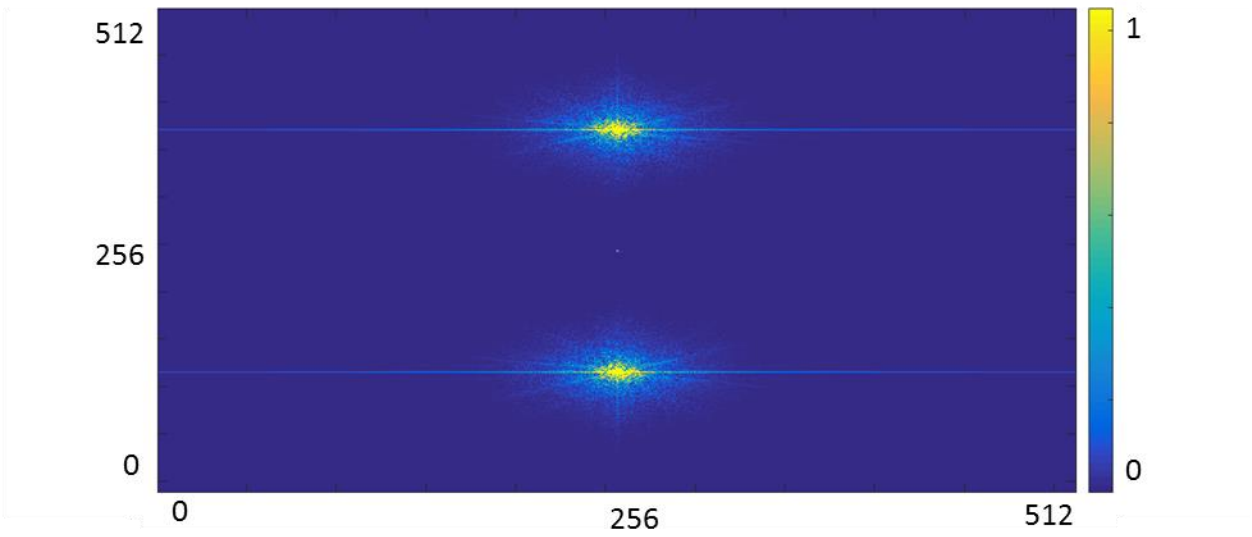

Figure 5 Hologram represented in the frequency domain.

The larger two regions are known from equation (3.5) to be the direct and conjugate terms of the hologram. Filtering the direct term from the others gives us Figure 6.

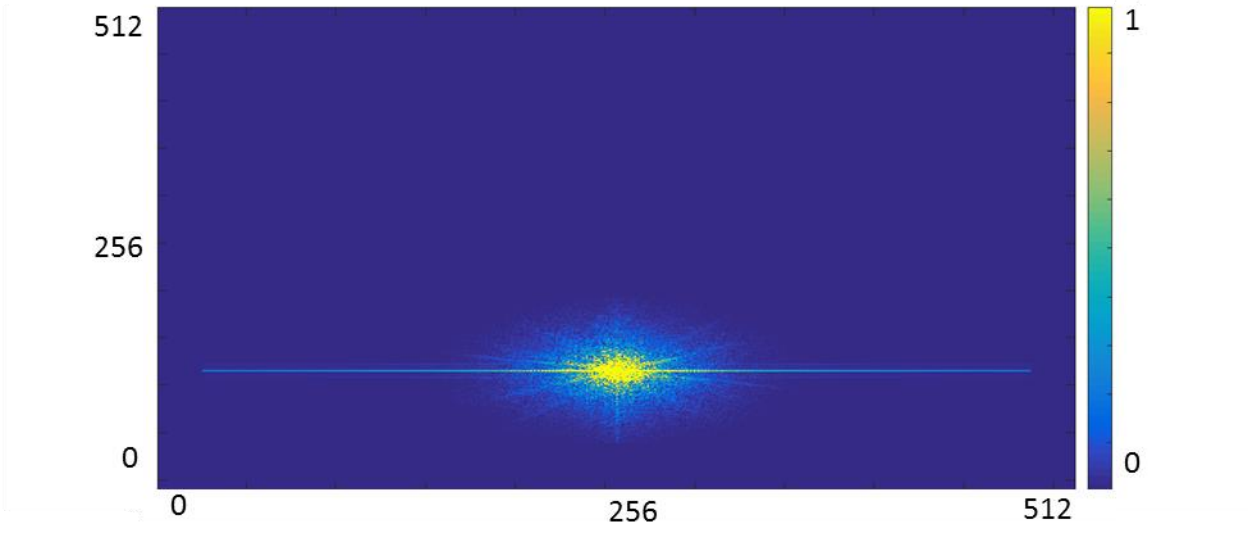

Figure 6 Direct term filtered from the hologram.

We take the inverse Fourier transform of the isolated direct term and then apply a phase shift of $\boldsymbol{k}_{||}$ to the hologram to result in the reconstruction of the original image. The reconstruction for our sample amplitude and phase images is revealed in Figure 7.

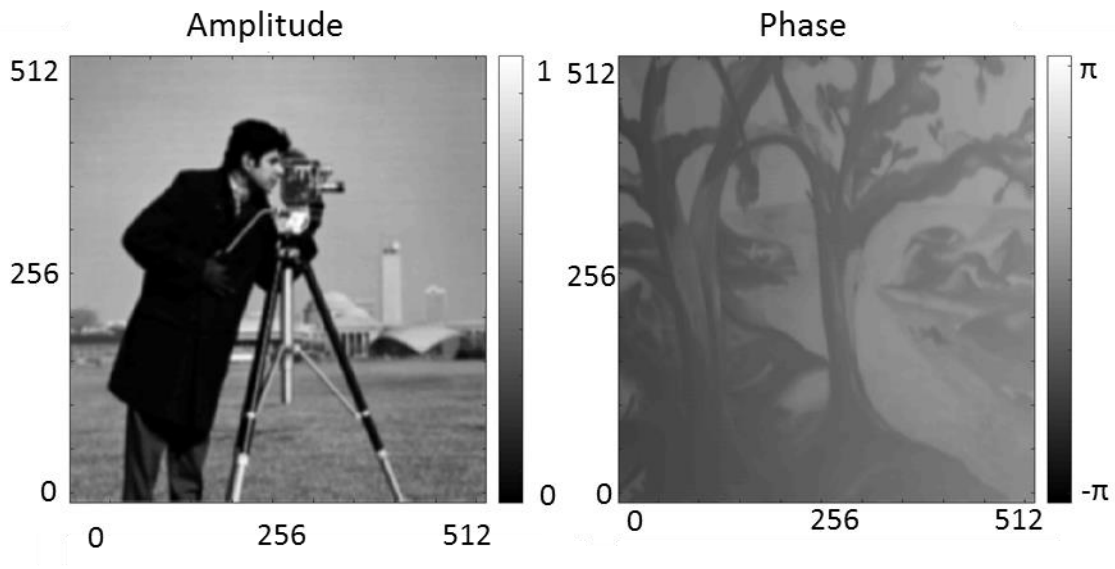

Figure 7 Image reconstruction.

Our simulation could be easily applied to real samples when provided with experimental data. The intensities recorded from the one-pixel detectors are read in as the hologram and from there, the program is able to compute the reconstruction of the sample.

4. Nonlinear-Phase Reference Waves

Synthetic optical holography with linear-phase reference waves provides the advantage of relative derivational simplicity at the cost of several key factors. Replacing linear movement of the piezo-actuated mirror with an oscillation about the zero-position in a sinusoidal motion instead produces a nonlinear-phase reference wave that matches the mirror movement. Using a sinusoidal-phase reference wave offers the benefits of shorter distances required for the piezo-actuator to travel with the mirror and an open-loop control system with no feedback needed between the mirror position and the scanning speed of the sample, as is needed in the linear-phase case [4].

4.1 Derivation

Generating a sinusoidal-phase reference wave produces a field shown as

$$U_R(t) = A_R e^{i\gamma \sin(2\pi f t + \phi)}, \tag{4.1}$$

where γ is the modulation amplitude, f is the oscillation frequency, and ϕ is the phase offset from the mirror zero position. By defining $\boldsymbol{k}_{||}$ as the wavevector in the sinusoidal case, we notice that the reference field can be expressed as a Jacobi-Anger expansion of plane-wave components,

$$U_{R,a,b} = A_R e^{i\gamma \sin(\boldsymbol{k}_{||}\cdot \boldsymbol{r} + \phi)} = A_R \sum_{n=-\infty}^{\infty} J_n(\gamma) e^{in(\boldsymbol{k}_{||}\cdot \boldsymbol{r} + \phi)}. \tag{4.2}$$

Squaring the field reveals an intensity of

$$I_{a,b} = \left|U_{S,a,b}(\boldsymbol{r})\right|^2 + |A_R|^2 + A_R U_{S,a,b}^* \sum_{n=-\infty}^{\infty} J_n(\gamma) e^{in\phi} e^{in\boldsymbol{k}_{||}\cdot \boldsymbol{r}_{a,b}} + c.c. \tag{4.3}$$

Taking the Fourier transform results in

$$\begin{aligned} \tilde{I}_{a,b} = \left|U_{S,a,b}(\boldsymbol{r})\right|^2 \delta_{p,q} + \tilde{C}_{p,q} + A_R \sum_{n=-\infty}^{\infty} J_n(\gamma) e^{in\phi} U_{S,nl_x-p,nl_y-q}^* \\ + A_R^* \sum_{m=-\infty}^{\infty} J_m(\gamma) e^{im\phi} U_{S,ml_x+p,ml_y+q}. \end{aligned} \tag{4.4}$$

Replacing $m \to -n$ and applying

$$J_{-n}(x) = (-1)^n J_n(x) \tag{4.5}$$

gives the Fourier transform of the intensity, as shown by

$$\tilde{I}_{p,q} = \left|U_{S,a,b}(\boldsymbol{r})\right|^2 \delta_{p,q} + \tilde{C}_{p,q} + \sum_{n=-\infty}^{\infty} J_n(\gamma) e^{in\phi} (A_R \tilde{U}^*_{S,nl_x-p,nl_y-q} + (-1)^n A^*_R U_{S,ml_x+p,ml_y+q}). \quad (4.6)$$

The constant background and autocorrelation terms can be filtered out, as in the linear-phase approach. The final term produces components of the hologram very different from the linear case. Each subsequent value of n is a real or imaginary term of the field depending on whether n is even or odd, respectively. The infinite series repeats real and imaginary components wrapping around the frequency domain with large drop-off in each succeeding term. The modulation depth affects the weighting of each term and the number of terms to use before truncation.

4.2 Results

Using the same images from Figure 3 for our test amplitude and phase images gives us a hologram as shown in Figure 8 when using a sinusoidal-phase reference phase.

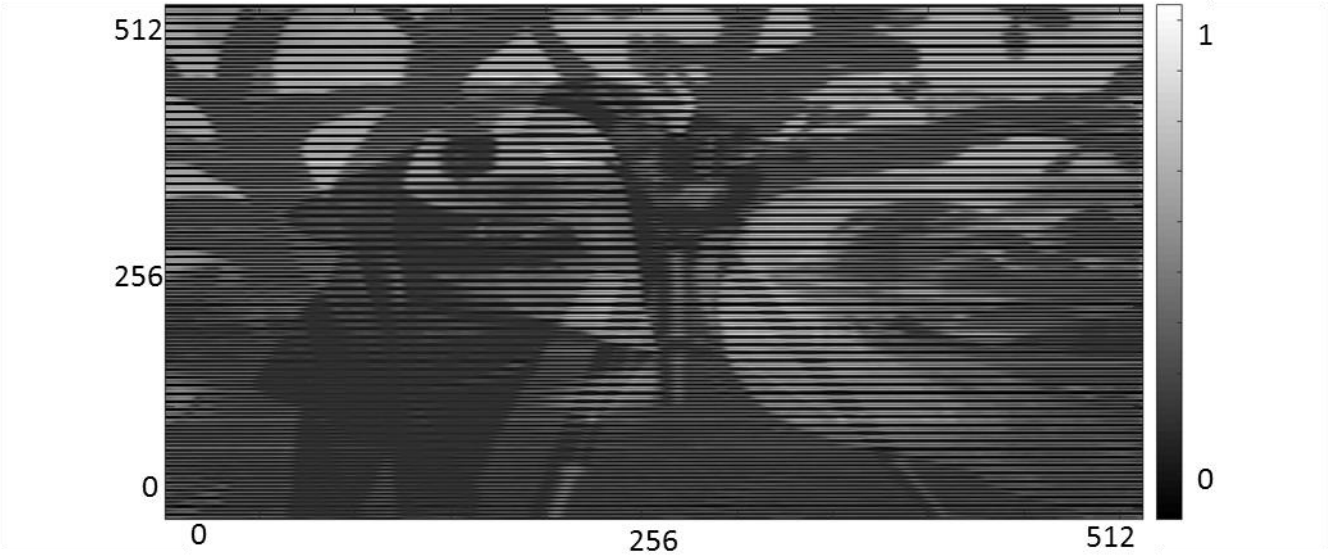

Figure 8 Hologram from image and sinusoidal-phase reference field.

The hologram data in the frequency domain is represented in Figure 9. The infinitely repeating terms are present wrapping around the edges of the domain. The number of lobes chosen to fit in the domain corresponds to the drop-off in amplitude of each successive component. The terms up to the fourth are sufficiently large that the spacing of the lobes is determined so that the fourth lobe lies on the boundary of the domain, in order to not overlap with any lobes of lower order that are to be filtered for the reconstruction.

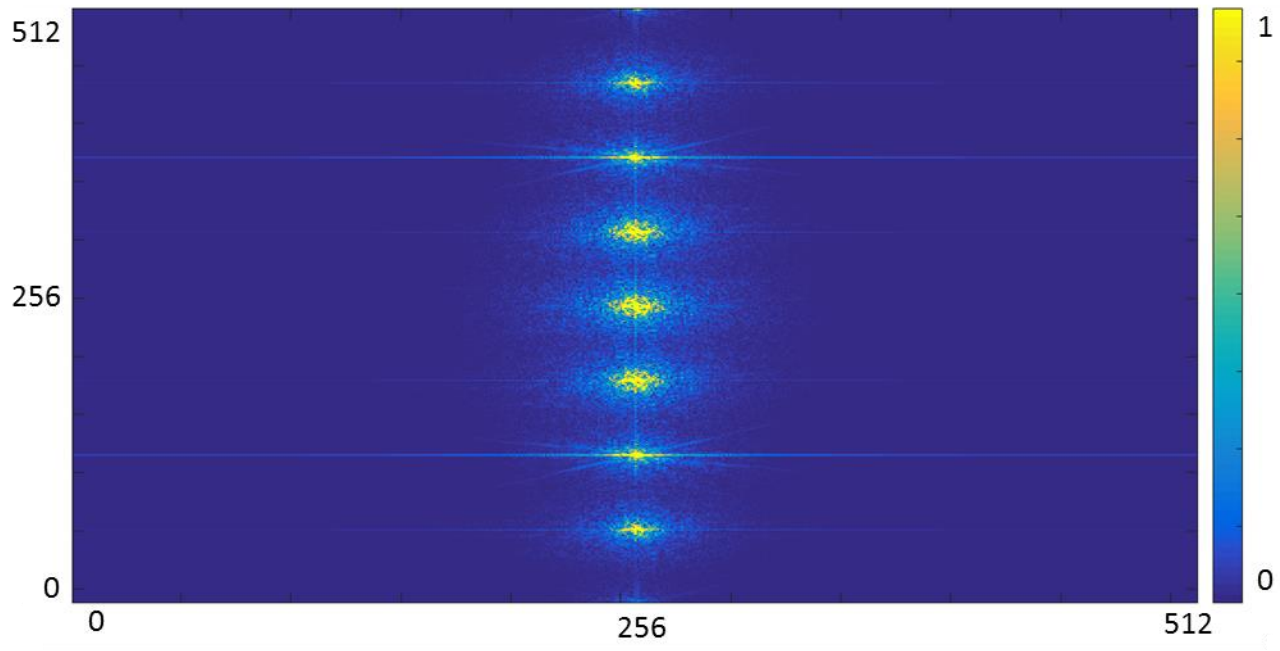

Figure 9 Hologram with infinitely repeating copies of real and imaginary components.

The first and second direct lobes are filtered out to represent the field's imaginary and real terms, respectively. Each term needs to be filtered out and shifted separately, as shown in Figure 10, in order to properly reconstruct the images.

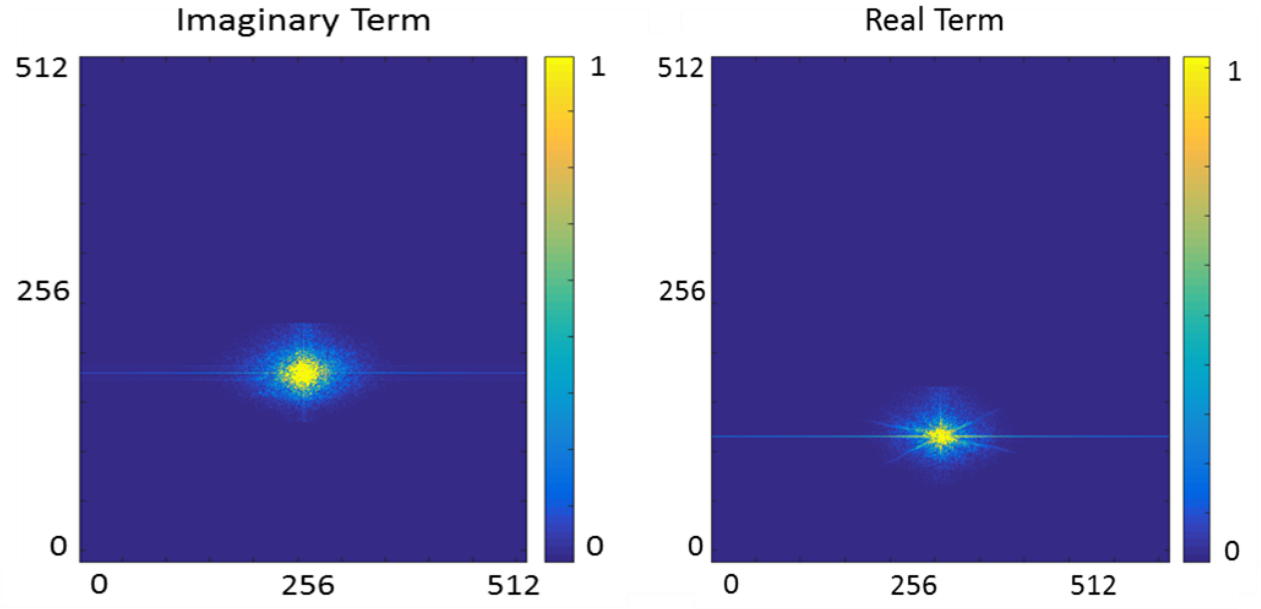

Figure 10 Filtered imaginary and real components of the hologram.

After shifting each term with the appropriate wavevector and combining the real and imaginary components correctly into amplitude and phase, the reconstruction of the original images is revealed in Figure 11.

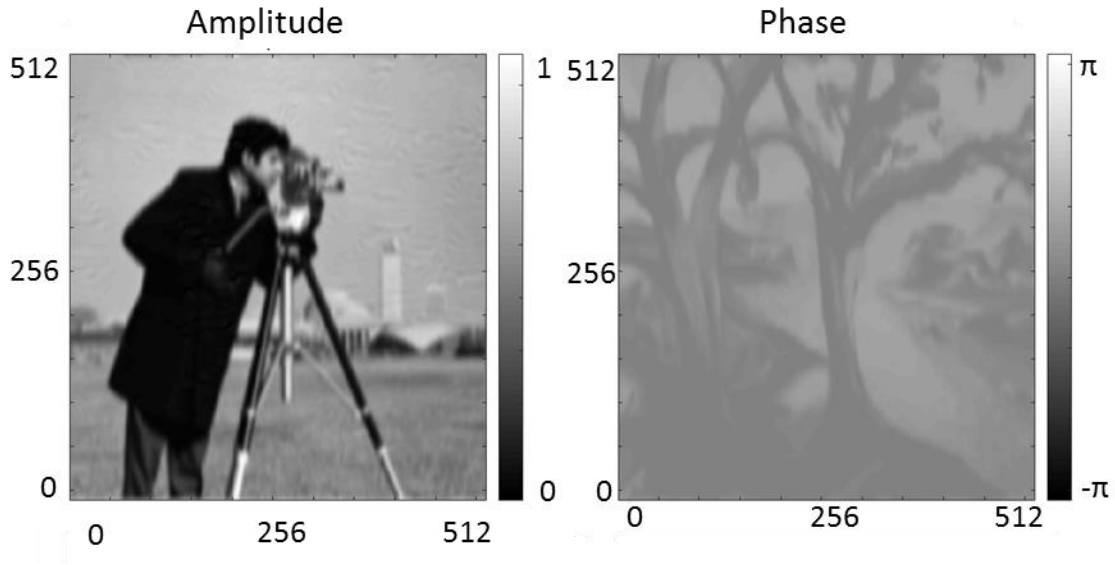

Figure 11 Reconstructed image.

5. Effects of Partial Coherence

After examining the image reconstructions in the linear and sinusoidal cases, we will look into the effects of coherence and broadening the bandwidth of our spectrum.

5.1 Degree of Coherence

Equation (3.7) shows us the relationship between the scattering field and reference field. Being more specific, the intensity seen at the detector is a time average of the incoming interference pattern. The relationship is revealed as

$$I(\boldsymbol{r}) = < |U_S(t) + U_R(t+\tau)|^2 >. \tag{5.1}$$

Solving for the intensity results in

$$I(\boldsymbol{r}) = < |U_S|^2 > + < |U_R|^2 > + < U_S^*(t)U_R(t+\tau) > + < U_S(t)U_R^*(t+\tau) >. \tag{5.2}$$

And introducing the scattering term, $K_R(\boldsymbol{r})$,

$$I(\boldsymbol{r}) = < |K_R(\boldsymbol{r})||U_R|^2 > + < |U_R|^2 > + < K_R^*(\boldsymbol{r})U_R^*(t)U_R(t+\tau) > + \\ < K_R(\boldsymbol{r})U_R(t)U_R^*(t+\tau) >. \tag{5.3}$$

Labeling $\Gamma(\tau) = < U_R^*(t)U_R(t+\tau) >$ as the mutual coherence function, we get

$$I(\boldsymbol{r}) = < |U_R|^2 > (|K_R(\boldsymbol{r})|^2 + 1) + K_R\big(\Gamma(\tau) + \Gamma^*(\tau)\big). \tag{5.4}$$

The mutual coherence function represents the temporal cross-correlation between the two fields. For self-coherence, the cross-correlation gives

$$\Gamma(\tau) = \int_0^\infty S(\omega)\, e^{-i\omega\tau} d\omega, \tag{5.5}$$

representing the Fourier transform of the spectral density, $S(\omega)$, with respect to frequency, ω [5].

The degree of coherence is a measure of the mutual coherence between two complex fields. The definition in relation to temporal coherence is

$$\gamma(\tau) = \frac{\Gamma_{12}(\tau)}{\sqrt{\Gamma_{11}(0)}\sqrt{\Gamma_{22}(0)}}, \tag{5.6}$$

For self-coherence, state 1 = state 2, leading to

$$\gamma(\tau) = \frac{\Gamma(\tau)}{\Gamma(0)}. \tag{5.7}$$

Using

$$I_j(\boldsymbol{r}) = \left|K_j(\boldsymbol{r})\right|^2 < \left|U(t-t_j)\right|^2 >, \tag{5.8}$$

equation (5.4) becomes

$$I(\boldsymbol{r}) = I_1(\boldsymbol{r}) + I_2(\boldsymbol{r}) + 2\sqrt{I_1(\boldsymbol{r})}\sqrt{I_2(\boldsymbol{r})}\,\Re\{\gamma(\tau)\}. \tag{5.9}$$

The real part of the degree of coherence, $\Re\{\gamma(\tau)\}$, is a value that can range from zero to one. The case of zero coherence means that the correlation term, $U_R^*(t)U_R(t+\tau)$, is able to take on significant values in a short period of time but cancels when taking the time average, $< U_R^*(t)U_R(t+\tau) > = 0$. This signifies random relative phases and complete incoherence, producing no interference patterns. When the time average is exactly one, the total system operates in the coherent limit and is completely coherent. Partial coherence is expected in actual application, where the coherence is greater than zero and less than one. This is the usual case for interference between the reference and sample fields, and is what we will be using for our simulation calculations.

Figure 12 shows several cases for various values of the degree of coherence, starting from complete coherence, $\Re\{\gamma(\tau)\} = 1$, to complete incoherence, $\Re\{\gamma(\tau)\} = 0$. Several cases of partial coherence, $0 < \Re\{\gamma(\tau)\} < 1$, are shown in between. The partial coherence terms shown in the figure are unusually low, intended to show the effects of diminishing coherence. Our normally used partial coherence terms produce a reconstruction much like that for complete coherence.

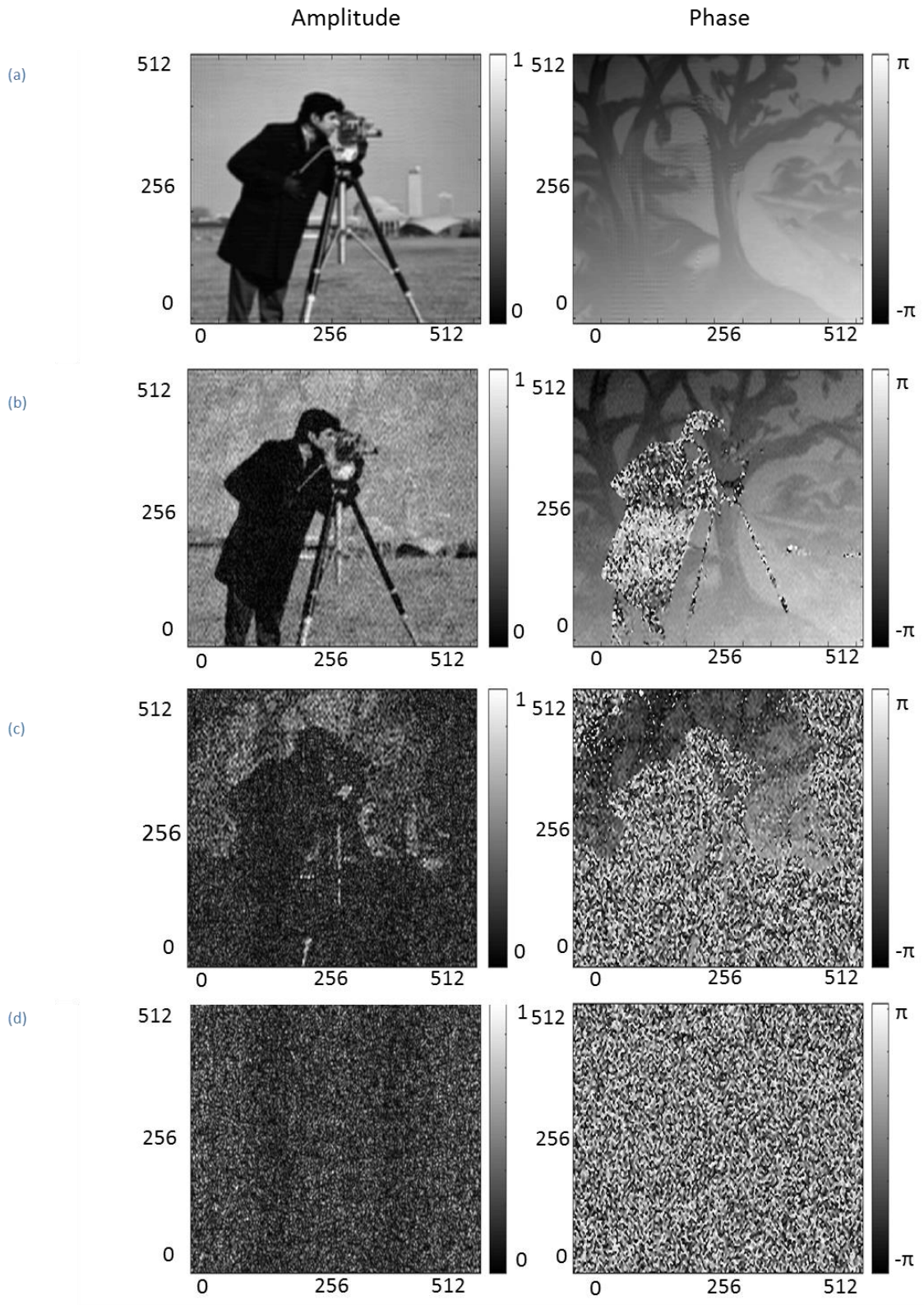

Figure 12 (a) Complete coherence. (b) Low partial coherence. (c) Extremely low partial coherence. (d) Complete incoherence.

5.2 Bandwidth Broadening

We next look at the effects of our source bandwidth. Our derivations assumed monochromatic (or quasi-monochromatic) sources, but true sources would have some determinable bandwidth. Increasing the bandwidth results in more loss of the reconstruction in the linear case, as revealed in Figure 13.

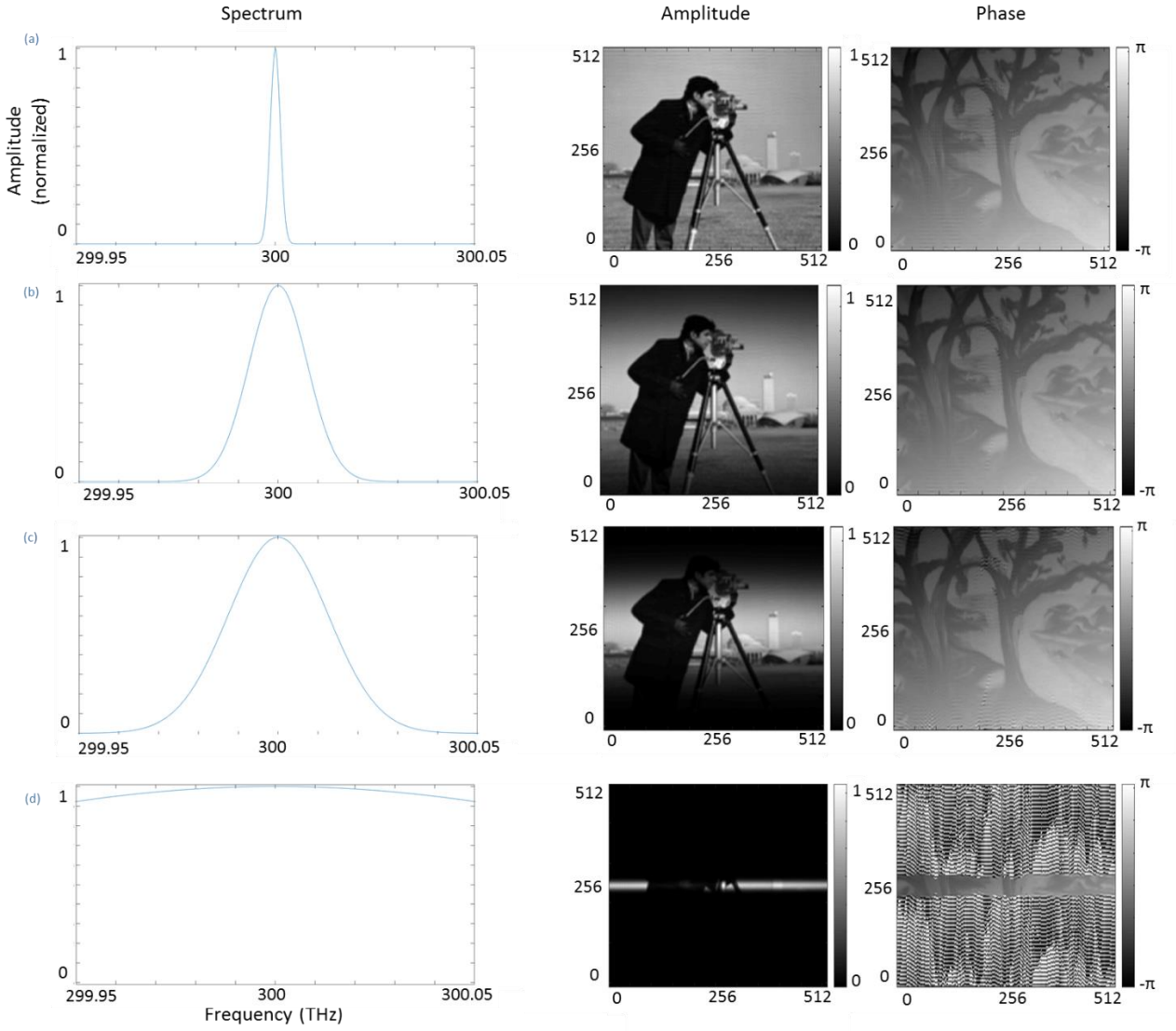

Figure 13 (a) Fine spectrum with clear results. (b) Slightly broader spectrum. (c) Even broader spectrum. (d) Broadest spectrum with drastically limited reconstruction.

Broadening the bandwidth around a fixed center frequency results in a darkening of the upper and lower edges of our reconstruction. The horizontal center of our image, dubbed the white-light point, retains the correct reconstruction while quickly dying off based on the amount of bandwidth broadening that was applied. We are able to account for this and recover the lost reconstruction by vertically shifting

the white-light point. Repeating the reconstruction process, another component of the image would be properly reconstructed. Iterating through enough changes in the white-light point could reproduce enough of the image that the reconstruction could be stitched together from the several reconstructions using the shifts in the white-light point.

The sinusoidal case has no such dependence on the bandwidth of the spectrum. This is revealed in Figure 14, as a very broad spectrum results in the exact same reconstruction for both the amplitude and phase. This suggests that the sinusoidal case does not depend on a white-light point. The piezo-controlled mirror can begin its translation at any point along the path and, as long as the motion is sinusoidal, the entire process can be open-loop with no feedback between the piezo-controlled mirror and the controller for sample detection position.

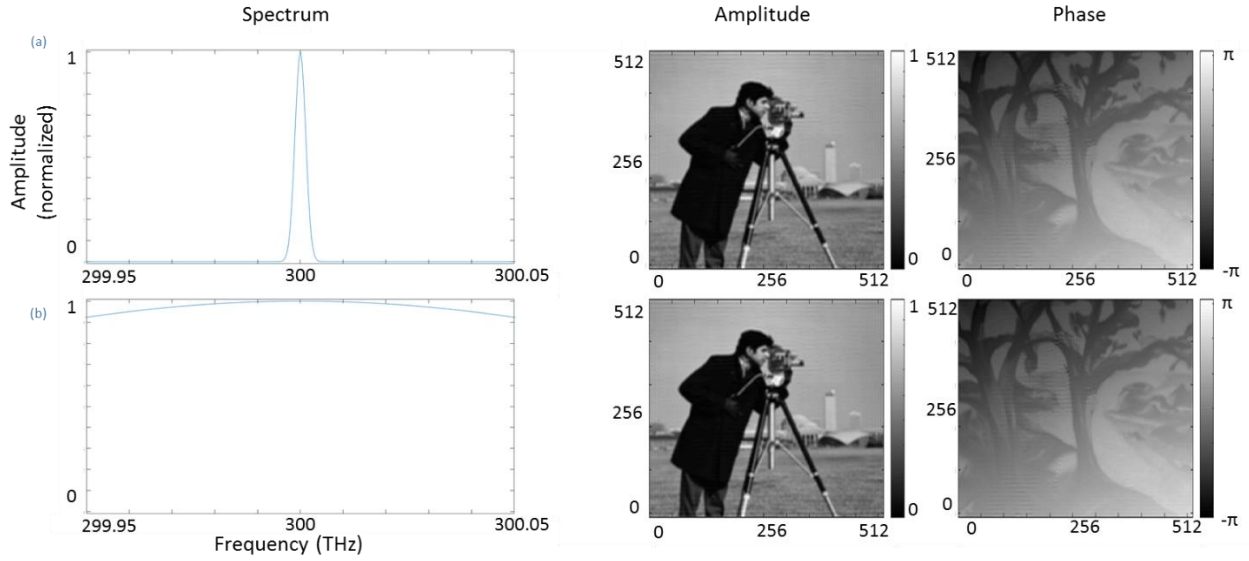

Figure 14 (a) Fine spectrum. (b) Broad spectrum results in the same reconstruction in the sinusoidal case.

5.3 Bichromatic Spectra

Verifying the results for monochromatic spectra, we then examine the linear case for a bichromatic spectral input. Synthetic optical holography is capable of simultaneous measurements with two sources of separate wavelengths. We will confirm this with our simulation. The bichromatic input and its resulting frequency domain interpretation of the hologram are shown in Figure 15. We notice a direct and conjugate term for each frequency that is used.

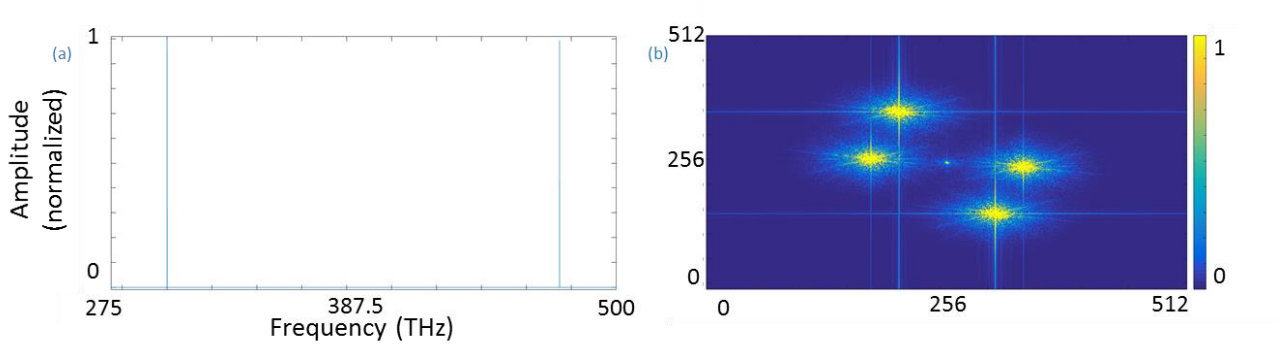

Figure 15 (a) Bichromatic spectrum. (b) Frequency domain of the resulting hologram.

Solving for the reconstruction, we see in Figure 16 that we can filter out the direct term of one frequency to obtain a reconstruction and separately filter out the direct term of the other frequency to obtain another full reconstruction. The original image in our simulation does not change depending on frequency, so both reconstructions are the same. Actual samples would show differing images based on various wavelengths, depending on the difference in wavelength.

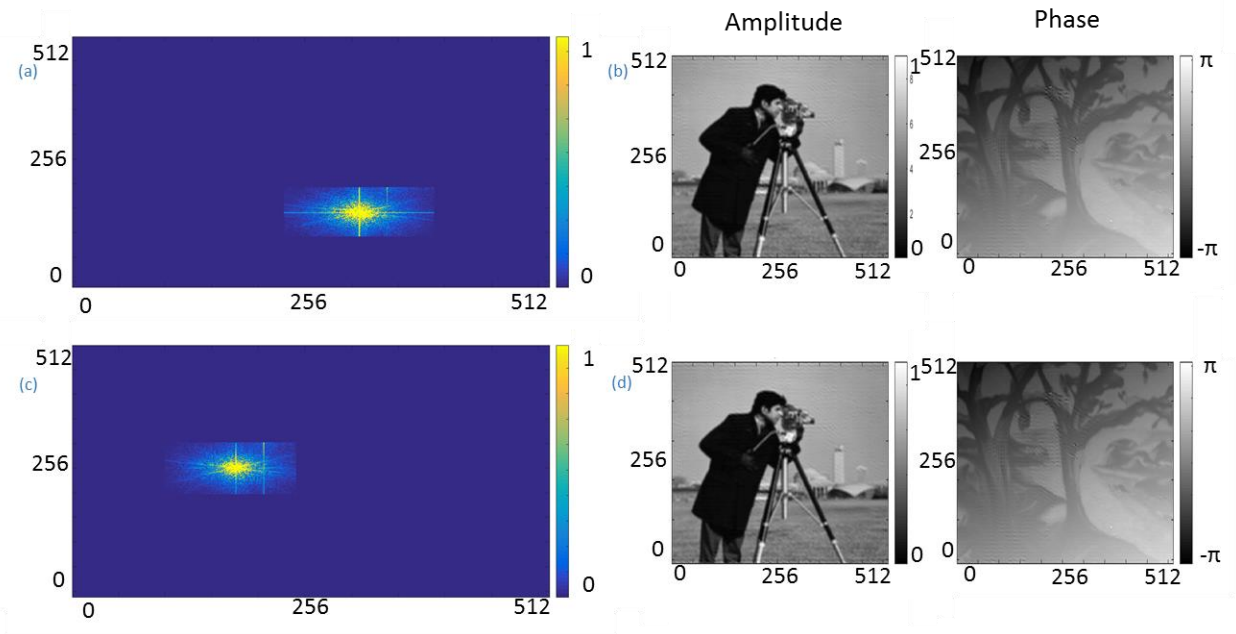

Figure 16 (a) Wavelength 1 direct term filtered. (b) Reconstruction due to wavelength 1. (c) Filtered hologram due to wavelength 2. (d) Reconstruction from wavelength 2, same as (b).

5.4 Real Spectra

Using all of this information, our next step was to apply our simulations to obtain reconstructions when using real spectral information from commercial devices. In Figure 17, we used a HeNe laser, LED, and

incoherent light bulb as sources for the linear-phase reference field case of our simulations. The bandwidth of the input field appears to have the predominant weight in affecting our reconstructions in the linear case.

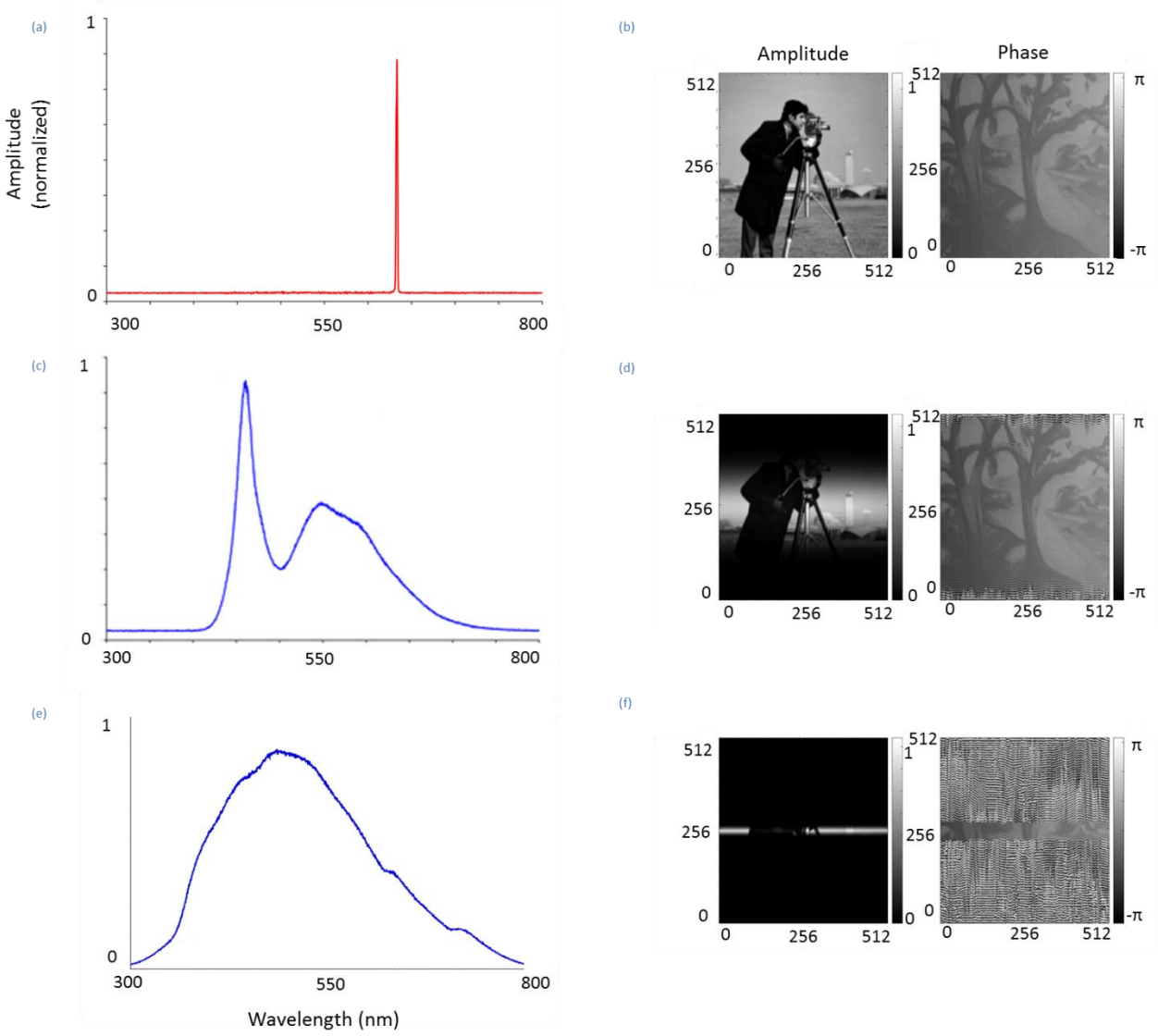

Figure 17 (a) Spectrum of HeNe laser. (b) Ideal reconstruction using HeNe. (c) Spectrum of input LED. (d) Slightly limited linear reconstruction from LED. (e) Light bulb spectrum. (f) Limited reconstruction due to light bulb.

We then looked at the sinusoidal case with the same input spectra. As revealed in Figure 18, the best reconstruction is also with the quasi-monochromatic HeNe input. The following reconstructions have artifacts due to the difficult filtering in the frequency domain of the sinusoidal case. Larger filtering windows introduce noise from the other terms, whereas smaller filtering results in less content for the reconstruction and a harsh blurring of the image. Using real spectra, we learn that the input can affect the

reconstruction in the sinusoidal case, not because of the bandwidth, but by affecting the direct and conjugate terms in the hologram frequency domain. The sinusoidal case is thus more prone to artifacts, but can be more effective in a particular application as long as care is taken in the handling of the hologram information.

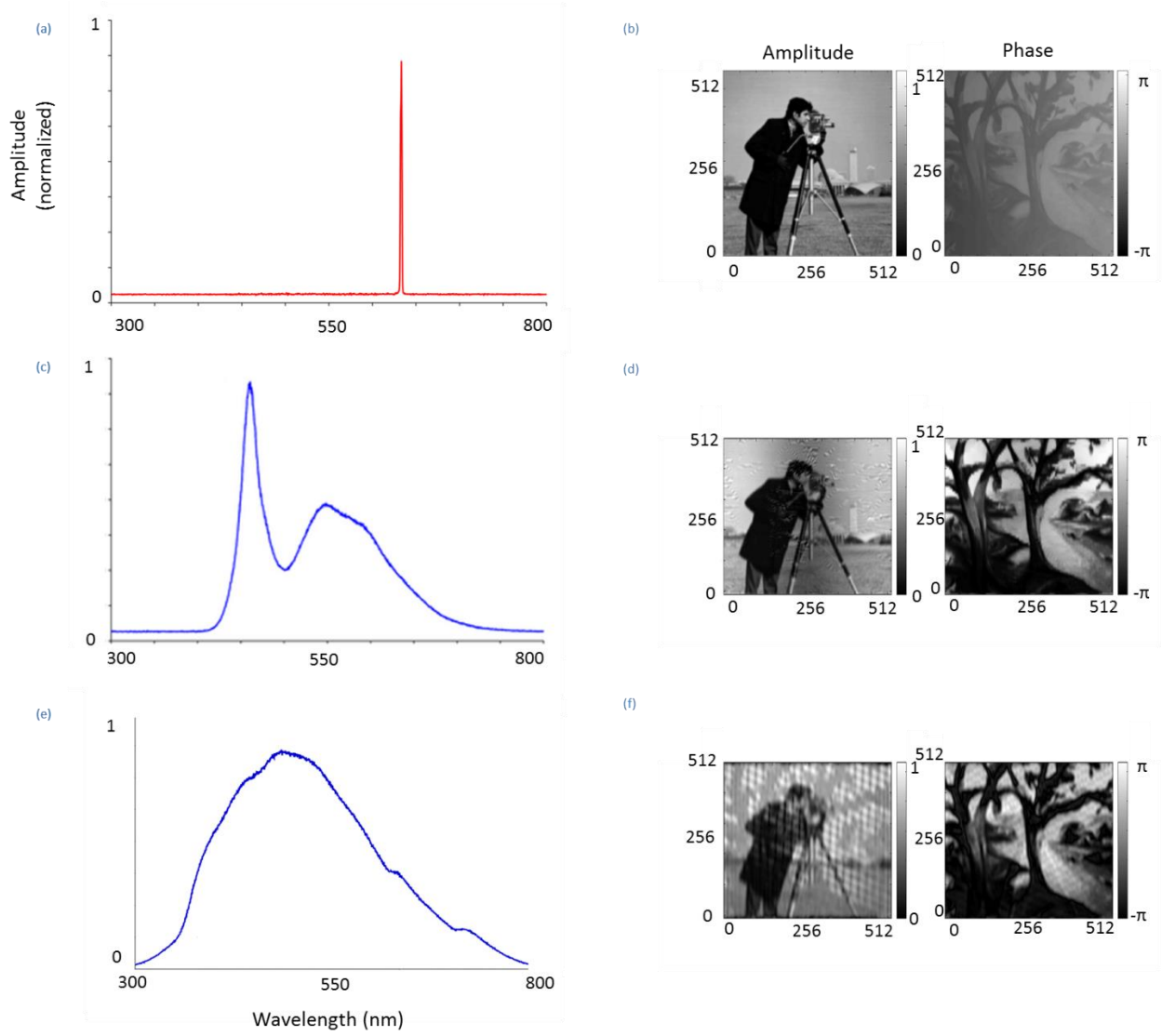

Figure 18 (a) Spectrum of HeNe laser. (b) Ideal reconstruction using HeNe. (c) Spectrum of input LED. (d) Sinusoidal reconstruction from LED. (e) Light bulb spectrum. (f) Limited reconstruction due to light bulb.

6. Conclusion

Synthetic optical holography is a powerful new method in implementing phase imaging in scanning near-field optical microscopy. This novel technique also finds applications in confocal microscopy, bio-imaging, and semiconductor manufacturing, among many others. New applications and innovative holographic encoding and reconstruction methods are highly anticipated.

Examining several cases and effects of synthetic optical holography, we inspected the linear and sinusoidal cases for translating the reference arm, which directly affected the phase of the reference field. We first derived and confirmed the results for the case of linear-phase reference waves. We then exposed the derivational complexity, along with experimental usefulness, of the sinusoidal-phase reference waves. With the data we have produced, we showed how the coherence and bandwidth influence our system and discussed plans to resolve these effects.

References

[1] U. Dürig, D. W. Pohl, and F. Rohner, "Near-field optical scanning microscopy," *Journal of Applied Physics,* vol. 59, no. 10, pp. 3318-3327, May 1986.

[2] M. Schnell, P. S. Carney, and R. Hillenbrand, “Synthetic optical holography for rapid nanoimaging,” *Nature Communications,* vol. 5, March 2014.

[3] M. Schnell, M. J. Perez-Roldan, P. S. Carney, and R. Hillenbrand, “Quantitative confocal phase imaging by synthetic optical holography,” *Optics Express*, vol. 22, pp. 15267-15276, June 2014.

[4] B. Deutsch, M. Schnell, R. Hillenbrand, and P. S. Carney, “Synthetic optical holography with nonlinear-phase reference,” *Optics Express*, vol. 22, pp. 26621-26634, Nov. 2014.

[5] S.K. Saha, *Aperture Synthesis: Methods and Applications to Optical Astronomy*, Springer Science + Business Media, 2011.